Astron. Astrophys. 239, 413–423 (1990)

ASTRONOMY AND ASTROPHYSICS

Nonlinear mean-field dynamo models: stability and evolution of three-dimensional magnetic field configurations

K.-H. Rädler[1], E. Wiedemann[1], A. Brandenburg[2], R. Meinel[1], and I. Tuominen[2]

[1] Sternwarte Babelsberg, Akademie der Wissenschaften, Rosa-Luxemburg-Str. 17a, 1591 Potsdam, German Democratic Republic
[2] Observatory and Astrophysics Laboratory, University of Helsinki, Tähtitorninmäki, SF-00130 Helsinki, Finland

Received July 2; accepted August 20, 1990

Abstract. The stability and evolution of three-dimensional magnetic field configurations of nonlinear mean-field dynamo models is investigated. Various models with isotropic and anisotropic α-effect are examined. The nonlinearity is due to α-quenching; the α-coefficient varies with the local energy density of the mean magnetic field. The dynamo number characterizing the strength of the α-effect is varied from marginal up to three times supercritical values. Two models with isotropic α-effect are studied, for which an axisymmetric solution (A0) is the marginal one. In these models a single stable solution showing the same symmetry is found. Furthermore, a model with anisotropic α-effect is investigated for which the marginal solution is known to be non-axisymmetric (S1). Correspondingly, for slightly supercritical dynamo numbers a non-axisymmetric solution is the only stable one. For dynamo numbers exceeding a certain (approximately two times supercritical) value also a stable axisymmetric solution (A0) is found. For even higher dynamo numbers the non-axisymmetric solution loses stability to the axisymmetric solution. Finally, a model with differential rotation is investigated in a parameter regime where four different modes are approximately equally excitable. Mixed parity solutions with periodic time dependence occur.

Key words: Hydromagnetics: mean-field dynamo – stability – non-axisymmetric magnetic fields – Sun and stars: magnetic fields

1. Introduction

There is a great number of investigations of dynamo models which provide some insight into the processes responsible for the existence of magnetic fields of the Earth, the planets, the Sun and other objects. Most of the models are elaborated only at the kinematic level, that is, the back-reaction of the magnetic field on the fluid motions is ignored. In this way one can determine the conditions under which states without any magnetic field become unstable and self-excitation of magnetic fields occurs. In order to study their further evolution, e.g., to determine the magnitude to which the fields may grow or details concerning their geometrical structure or time behaviour, the back-reaction has to be taken into account.

In view of the cosmical objects mentioned steady states are of particular interest. The stability of these states determines which of them may be expected to be realized in nature (cf. Krause and Meinel, 1988). In general, only stable configurations are relevant for explaining magnetic fields in cosmical objects. Of course, it may be possible that the time scale of an instability is rather long. In this case an unstable magnetic field configuration, that has been built up due to any circumstances in the past, may be observed within the subsequent life time of the object.

Investigating a model at the kinematic level means considering the induction equation governing the magnetic field with given fluid motion. Then the problem to be solved is linear. If the back-reaction of the magnetic field on the motion is included we are faced with the full set of magnetohydrodynamic equations and thus with a complex nonlinear problem.

In the framework of mean-field dynamo theory some attempts have been made to approach this problem by investigating only the induction equation in which this back-reaction is taken into account in a crude way; see, e.g. Braginski (1970), Stix (1972), Rüdiger (1973), Jepps (1975), Ivanova and Ruzmaikin (1977) and Rädler (1984). A dependence of the α-coefficient or related quantities on the magnetic field has been allowed and specified by simple assumptions.

In this paper we report on numerical experiments with mean-field dynamo models of that kind. Our numerical code is not restricted to axisymmetric fields. In this way we are able to clarify in some cases whether or not the results by Brandenburg et al. (1989a), which have been obtained by considering axisymmetric fields only, remain valid within this general frame. As already shown by Rädler and Wiedemann (1989), some results concerning the stability of axisymmetric fields have to be modified if non-axisymmetric perturbations are allowed.

2. The model

We consider a traditional spherical mean-field dynamo model. Let the rotating spherical body of electrically conducting fluid be surrounded by free space. The mean magnetic flux density, $\boldsymbol{B}$, is assumed to obey the induction equation

Send offprint requests to: K.-H. Rädler

$$\frac{\partial \boldsymbol{B}}{\partial t} = \eta \Delta \boldsymbol{B} + \operatorname{curl}(\mathscr{E} + \boldsymbol{u} \times \boldsymbol{B}) \tag{1}$$

inside the body and to continue as an irrotational field outside. The magnetic diffusivity η is taken as constant. As for the mean electromotive force due to fluctuations, $\mathscr{E}$, we restrict ourselves to the α-effect, that is

$$\mathscr{E} = \alpha \boldsymbol{B}. \tag{2}$$

In addition to examples of an isotropic α-effect, in which α is a scalar, we will deal below also with a special case of an anisotropic α-effect, in which α is a tensor. As for the mean motion a differential rotation is allowed. In that sense the mean velocity $\boldsymbol{u}$ is specified as

$$\boldsymbol{u} = \Omega \hat{\boldsymbol{z}} \times \boldsymbol{r}, \tag{3}$$

where Ω denotes the angular velocity which may depend on radius and latitude, $\hat{\boldsymbol{z}}$ the unit vector parallel to the axis of rotation and $\boldsymbol{r}$ the radius vector.

The fluctuating motions which are responsible for the α-effect as well as the mean motion are in general influenced by the magnetic field. Without studying this back-reaction of the magnetic field on the motions in detail we take it partly into account by a simple assumption on the dependence of α on $\boldsymbol{B}$. Further feedback effects which lead to a modification of other mean-field coefficients (e.g. the turbulent magnetic diffusivity) and, in particular, of the mean motion are neglected. We hope that, nevertheless, our study comprises some important aspects of the nonlinear dynamo regime.

For α we put

$$\alpha = \alpha_0 f(e), \quad e = \frac{1}{2\mu}\boldsymbol{B}^2, \tag{4}$$

where α_0 is independent of $\boldsymbol{B}$, and f a function of e, and μ the permeability of free space; e can be interpreted as the local energy density of the mean magnetic field. We suppose $f(0) = 1$, $f(e) \geq 0$, and we will specify f so that it decreases with growing e.

Following the traditional concept of spherical mean-field dynamo models we assume simple symmetry properties of α_0 with respect to equatorial plane and axis of rotation. In the cases of isotropic α-effect, α_0 is a scalar which is antisymmetric about the equatorial plane and symmetric about the axis of rotation. For the anisotropic α-effect an analogous assumption is made which will be formulated below. The angular velocity Ω is symmetric about the equatorial plane and the axis of rotation.

We may decompose any $\boldsymbol{B}$-field into two parts that are symmetric or antisymmetric about the equatorial plane, and either part into its Fourier components with respect to the azimuthal coordinate. In that sense we consider $\boldsymbol{B}$ in the following as a superposition of contributions $\boldsymbol{B}^m_{\mathrm{A}}$ and $\boldsymbol{B}^m_{\mathrm{S}}$ which have the form

$$\boldsymbol{B}^m_{\mathrm{A,S}} = \operatorname{Re}[\boldsymbol{C}^m_{\mathrm{A,S}} \exp(\mathrm{i}m\phi)], \tag{5}$$

where $\boldsymbol{C}^m_{\mathrm{A}}$ and $\boldsymbol{C}^m_{\mathrm{S}}$ are complex vector fields that are antisymmetric or symmetric about the equatorial plane and symmetric about the axis of rotation, m is a non-negative integer, and ϕ the azimuthal coordinate. Adopting the usual notation we will speak in the following of Am or Sm parts, or Am or Sm fields.

In the limit of vanishing magnitude of $\boldsymbol{B}$ we have $f = 1$, and our model turns into a kinematic, that is, linear model. In this case the general solution of the equations governing $\boldsymbol{B}$ is a superposition of independent modes, $\boldsymbol{B}_i$, of the form

$$\boldsymbol{B}_i = \operatorname{Re}(\hat{\boldsymbol{B}}_i e^{\lambda_i t}), \tag{6}$$

where $\hat{\boldsymbol{B}}_i$ depends only on position and λ_i is a complex constant. Due to our assumptions concerning the symmetries of α and Ω these $\boldsymbol{B}$-modes show again simple symmetries. Each such $\boldsymbol{B}$-mode has just the form of a single $\boldsymbol{B}^m_{\mathrm{A}}$ or $\boldsymbol{B}^m_{\mathrm{S}}$, that is, it is simply an Am or Sm mode.

For finite magnitudes of $\boldsymbol{B}$, however, we are faced with a more complex nonlinear problem. The dependence of α on position is no longer determined by α_0 only but, via f, also by $\boldsymbol{B}$. Therefore α will in general no longer show the symmetries of α_0, and this leads to couplings between individual Am and Sm fields. However, because of the dependence of f on $\boldsymbol{B}^2$ only there are solutions which do not contain the whole spectrum of Am and Sm fields. Among them are solutions which can be regarded as natural extensions of the Am and Sm solutions of the linear problem. We denote them by $\mathscr{A}m$ and $\mathscr{S}m$. Their structure is defined by

$$\begin{aligned}
&\mathscr{A}0: \ \mathrm{A}0\\
&\mathscr{S}0: \ \mathrm{S}0\\
&\mathscr{A}1: \ \mathrm{A}1 + \mathrm{A}3 + \mathrm{A}5 + \ldots\\
&\mathscr{S}1: \ \mathrm{S}1 + \mathrm{S}3 + \mathrm{S}5 + \ldots\\
&\mathscr{A}2: \ \mathrm{A}2 + \mathrm{A}6 + \mathrm{A}10 + \ldots\\
&\mathscr{S}2: \ \mathrm{S}2 + \mathrm{S}6 + \mathrm{S}10 + \ldots\\
&\mathscr{A}3: \ \mathrm{A}3 + \mathrm{A}9 + \mathrm{A}15 + \ldots\\
&\mathscr{S}3: \ \mathrm{S}3 + \mathrm{S}9 + \mathrm{S}15 + \ldots
\end{aligned} \tag{7}$$

In contrast to the situation in the linear problem, superpositions of such solutions are not solutions of the nonlinear problem.

In general, the geometrical structures of the solutions $\boldsymbol{B}$ of our problem will be more complex as in the case of the special solutions considered so far. This holds in particular if we follow the evolution of a magnetic field containing initially an arbitrary mixture of Am and Sm parts. We will pay special attention to the structure of the field in the final state of evolution. If it corresponds to an $\mathscr{A}m$ or $\mathscr{S}m$ solution as defined by (7), we speak of "pure states" or "pure solutions", otherwise of "mixed states" or "mixed solutions". It should be stressed that a mixed solution cannot be considered as a linear superposition of pure solutions.

When analysing the magnetic fields which occur as solutions of our problem we will in particular deal with the parts $\boldsymbol{B}_{\mathrm{A}}$ and $\boldsymbol{B}_{\mathrm{S}}$ that are antisymmetric or symmetric about the equatorial plane,

$$\boldsymbol{B}_{\mathrm{A,S}} = \sum_m \boldsymbol{B}^m_{\mathrm{A,S}}, \tag{8}$$

and with the spectrum of the Fourier components $\boldsymbol{B}^m$ with respect to the azimuthal coordinate,

$$\boldsymbol{B}^m = \boldsymbol{B}^m_{\mathrm{A}} + \boldsymbol{B}^m_{\mathrm{S}}. \tag{9}$$

We will also consider the parts $\boldsymbol{B}_{\mathrm{D}}$ and $\boldsymbol{B}_{\mathrm{Q}}$ which comprehend the constituents belonging to the dipole and quadrupole family, respectively, that is,

$$\boldsymbol{B}_D = \boldsymbol{B}_A^0 + \boldsymbol{B}_A^2 + \ldots + \boldsymbol{B}_S^1 + \boldsymbol{B}_S^3 + \ldots$$
$$\boldsymbol{B}_Q = \boldsymbol{B}_S^0 + \boldsymbol{B}_S^2 + \ldots + \boldsymbol{B}_A^1 + \boldsymbol{B}_A^3 + \ldots \quad (10)$$

Finally, we will also consider the poloidal and toroidal parts, $\boldsymbol{B}_P$ and $\boldsymbol{B}_T$.

In the following we characterize the magnitudes of the $\boldsymbol{B}$-field or its various parts by energies. The total energy, E, of the $\boldsymbol{B}$-field is defined by

$$E = \frac{1}{2\mu} \int \boldsymbol{B}^2 dV, \quad (11)$$

where the integral is taken over the whole space, i.e., over the fluid body and outer space. Analogously we define energies E_A^m, E_S^m, E_A, E_S, E^m, E_D, E_Q, E_P, and E_T for the respective parts of the total field, $\boldsymbol{B}_A^m$, $\boldsymbol{B}_S^m$, $\boldsymbol{B}_A$, $\boldsymbol{B}_S$, ... The energy to be ascribed to a sum of such parts, e.g. E_A^m and E_S^m, is just equal to the sum of the energies of these parts.

Following the notation of Brandenburg et al. (1989a), we define a measure P of the degree of symmetry or antisymmetry of a $\boldsymbol{B}$-field about the equatorial plane by

$$P = \frac{E_S - E_A}{E_S + E_A}. \quad (12)$$

Clearly, $-1 \leq P \leq +1$, and $P = 1$ means complete symmetry, $P = -1$ complete antisymmetry. We also define a measure M for the deviation of a $\boldsymbol{B}$-field from symmetry about the axis of rotation by

$$M = 1 - E^0/E. \quad (13)$$

Then $0 \leq M \leq 1$, where $M = 0$ corresponds to complete axisymmetry of the $\boldsymbol{B}$-field and $M = 1$ to the absence of any axisymmetric parts. We further define a quantity Q which indicates the proportion of constituents of a $\boldsymbol{B}$-field that belong to the dipole or quadrupole family,

$$Q = \frac{E_D - E_Q}{E_D + E_Q}. \quad (14)$$

Thus $-1 \leq Q \leq +1$, and $Q = 1$ or $Q = -1$ mean that all constituents belong to the dipole or quadrupole family, respectively.

3. The numerical method

The computations that we report in the following have been carried out with a program developed by Rädler and Wiedemann (1989). It allows us to follow the evolution of the magnetic field in spherical dynamo models as described above. When explaining the basic idea we rely again on equation (1), but with $\mathscr{E} + \boldsymbol{u} \times \boldsymbol{B}$ replaced by $\boldsymbol{F}$, and, imaging the usual non-dimensional quantities, suppose η to be replaced by 1. The basic idea is valid for quite general assumptions concerning the dependence of $\boldsymbol{F}$ on $\boldsymbol{B}$.

The program is based on an expansion of $\boldsymbol{B}$ in an infinite series,

$$\boldsymbol{B}(\boldsymbol{x}, t) = \sum b_i(t) \hat{\boldsymbol{B}}_i(\boldsymbol{x}), \quad (15)$$

and the reduction of the equations governing $\boldsymbol{B}$ to an infinite set of ordinary differential equations for the coefficients b_i. The vector functions $\hat{\boldsymbol{B}}_i$ correspond to the modes of free decay, that is, the fields $\hat{\boldsymbol{B}}_i(x)e^{\lambda_i t}$, with proper λ_i, satisfy the equations governing $\boldsymbol{B}$ in the case $\boldsymbol{F} = 0$. These $\hat{\boldsymbol{B}}_i$ form, for our problem, a complete set of functions. Each of them satisfies $\Delta \hat{\boldsymbol{B}}_i - \lambda_i \hat{\boldsymbol{B}}_i = 0$. Taking into account these properties of the $\hat{\boldsymbol{B}}_i$ we may reduce the equations for $\boldsymbol{B}$ to

$$\frac{db_i}{dt} = \lambda_i b_i + f_i, \quad (16)$$

where f_i, for each fixed i, is a function of all b_j, $j = 1, 2, 3, \ldots$ This function is defined by an integral over the fluid body. Its integrand depends on $\boldsymbol{F}(\boldsymbol{B})$, where $\boldsymbol{B}$ can be expressed according to (15). In general, of course, the integration cannot be carried out analytically, so that an explicit form of the relations between the f_i and the b_j is not available. For the numerical computations the expansion (15) of $\boldsymbol{B}$ is truncated, that is, only a finite number of terms is considered. Accordingly, only a finite set of equations of type (16) for the b_i is solved. This set is integrated by a modified second order Runge-Kutta method. In each time step the integrals defining the f_i are computed numerically. Apart from the choice of the time steps the accuracy of the results obtained in this way depends on the level of truncation of the expansion for $\boldsymbol{B}$ and on the accuracy of the determination of these integrals.

In order to describe the expansion (15) of $\boldsymbol{B}$ in more detail we first replace the index i by the quadruple (α, n, m, ℓ), that is, b_i and $\hat{\boldsymbol{B}}_i$ by $b_{n\ell}^{\alpha m}$ and $\boldsymbol{B}_{n\ell}^{\alpha m}$, and we interprete the $b_{n\ell}^{\alpha m}$ and $\boldsymbol{B}_{n\ell}^{\alpha m}$ in the usual way as complex quantities. The index α is introduced to distinguish between poloidal and toroidal fields. Accordingly it may take the values P or T. We then have

$$\boldsymbol{B}_{n\ell}^{Pm} = -\mathrm{curl}\,(\boldsymbol{r} \times \nabla S_{n\ell}^{Pm}), \quad \boldsymbol{B}_{n\ell}^{Tm} = -\boldsymbol{r} \times \nabla S_{n\ell}^{Tm} \quad (17)$$

$$S_{n\ell}^{\alpha m} = \psi_{n\ell}^{\alpha}(x) P_n^{|m|}(\cos\theta) e^{im\phi}, \quad \text{for} \quad x \leq 1, \quad (18)$$

where $\boldsymbol{r}$ is again the radius vector, x a dimensionless radial coordinate, the $\psi_{n\ell}^{\alpha}$ are functions which can easily be expressed by Bessel functions with half-integer index, and the P_n^m Legendre polynomials. The indices n, m, and l are subject to the conditions $n \geq 1$, $|m| \leq n$, and $l \geq 1$. Our truncation of (15) is given by $n \leq n_e$, $|m| \leq m_e$, and $l \leq l_e$, that is, defined by the three parameters n_e, m_e and l_e.

The determination of $f_{n\ell}^{\alpha m}$ can be reduced to the computation of integrals of the type

$$\int_0^1 dx\, x^2 \int_0^\pi d\theta\, \sin\theta \int_0^{2\pi} d\phi\, [\boldsymbol{r} \cdot \mathrm{curl}\, \boldsymbol{F}(\boldsymbol{B})](S_{n\ell}^{Pm})^* \quad (19)$$

and

$$\int_0^1 dx\, x^2 \int_0^\pi d\theta\, \sin\theta \int_0^{2\pi} d\phi\, [\boldsymbol{r} \cdot \mathrm{curl\,curl}\, \boldsymbol{F}(\boldsymbol{B})](S_{n\ell}^{Tm})^*, \quad (20)$$

where the asterisk denotes complex conjugation. The x, θ and ϕ integrals have been computed by the the Simpson or trapezium rule for sets of equidistant grid points. In the following, the number of intervals used for the x, θ and ϕ integrations is denoted by i_x, i_θ and i_ϕ, respectively.

4. Results for α^2-dynamo models

4.1. Specification of the models

In the following we present results for three different models of α^2-type. Models (i) and (ii) are those already investigated by Brandenburg et al. (1989a) and by Rädler and Wiedemann (1989), respectively, and model (iii) is a modification of the latter.

In models (i) and (ii) an isotropic α-effect, that is, a scalar α_0 is assumed. In both cases

$$\alpha_0 = a(\hat{\boldsymbol{z}} \cdot \hat{\boldsymbol{r}}) = a\cos\theta, \tag{21}$$

where a depends on radius only, $\hat{\boldsymbol{z}}$ is again the unit vector in the axial direction, $\hat{\boldsymbol{r}}$ that in the radial direction, and θ is the colatitude. Model (i) is defined by

$$a = \text{const} \geq 0, \tag{22}$$

and model (ii) by

$$a = a_c \begin{cases} \frac{15}{16}\frac{1}{d_a}(1-\xi_a^2)^2, & \text{for } |\xi_a| \leq 1, \quad \xi_a = \frac{x-x_a}{d_a}, \\ 0 \quad \text{elsewhere} \end{cases} \tag{23}$$

where a_c is a non-negative constant, $x = r/R$ with r being the radial coordinate and R the radius of the conducting sphere, and $x_a = d_a = 0.5$. We note that model (i) implies an ambiguity of α_0 at $r = 0$, which, however, does not influence the results.

In model (iii) an anisotropic α-effect, i.e. a tensorial α_0, is assumed. A special anisotropy is considered which is given by

$$(\alpha_0)_{ij} = a[(\hat{\boldsymbol{z}} \cdot \hat{\boldsymbol{r}})\delta_{ij} + \epsilon(\hat{z}_i\hat{r}_j + \hat{z}_j\hat{r}_i)]. \tag{24}$$

In this case $\alpha_0 \boldsymbol{B}$ takes the form

$$a\{(\hat{\boldsymbol{z}} \cdot \hat{\boldsymbol{r}})\boldsymbol{B} + \epsilon[(\hat{\boldsymbol{z}} \cdot \boldsymbol{B})\hat{\boldsymbol{r}} + (\hat{\boldsymbol{r}} \cdot \boldsymbol{B})\hat{\boldsymbol{z}}]\}.$$

Again, a is specified by Eq. (23) with $x_a = d_a = 0.5$. Clearly, model (iii) would coincide with model (ii) for $\epsilon = 0$. We fix, however, model (iii) by choosing $\epsilon = -0.25$.

For all three models we define a dimensionless measure C_α for the magnitude of the α-effect by

$$C_\alpha = \frac{1}{\eta}\int_0^R a(r)dr. \tag{25}$$

Furthermore, we assume the mean motion to be a rigid body rotation and refer to a corotating frame of reference so that

$$\boldsymbol{u} = 0. \tag{26}$$

The function f, which comprises the back-reaction of the magnetic field on the fluid motion responsible for the α-effect, is specified by

$$f = (1 + e/e_c)^{-1} \tag{27}$$

with some constant energy density e_c. The dependence of f on e is somewhat arbitrary; it recognizes only that f should vanish with growing e. We note that Rüdiger (1974) found under special assumptions that $\alpha = O(|\boldsymbol{B}|^{-3})$ for $|\boldsymbol{B}| \to \infty$.

For our numerical investigations of these models it proved to be sufficient to choose for n_e and l_e values of 8 to 10, for m_e of 3 to 5, for i_x and i_θ values of about 30, and for i_ϕ about 10. In several examples the accuracy has been checked by using higher values.

4.2. The linear case

Let us first look at our models in the linear case, for which $f = 1$. Table 1 containes the marginal values of C_α for the most easily excitable modes. In models (i) and (ii) the A0 mode, i.e. an axisymmetric mode, is favoured over all other modes, and it is followed by the S1 mode. Model (iii), however, has been chosen as an example in which the S1 mode, i.e. a non-axisymmetric mode, plays the dominating role, followed by the A0 mode.

Table 1. Marginal values C_α of the most easily excitable modes and the rotation rates ω of the non-axisymmetric field configurations for the α^2-dynamo models (i), (ii), and (iii). Positive ω means eastward, negative ω westward rotation

	A0	S0	A1		S1	
model	C_α	C_α	C_α	ω	C_α	ω
(i)	**7.64**	7.81	7.99	+0.89	7.66	+2.23
(ii)	**5.33**	5.44	5.55	−0.07	5.41	+2.01
(iii)	6.72	7.09	6.72	+0.03	**6.43**	+3.83

4.3. Pure solutions

We have looked for steady $\mathscr{A}m$ and $\mathscr{S}m$ fields. In this context, steadiness of fields is understood in a wider sense so that it also applies to fields which rotate like a rigid body, that is, they become steady in the strict sense only if a correspondingly rotating frame of reference is used. Starting from initial fields of appropriate symmetries we followed up their evolution. We have found indeed that the evolution approaches states in which not only the total energy E of the field but also the energies E_A^m and E_S^m of its Am or Sm parts no longer vary with time. Then there are good reasons to assume, and it has been checked in several examples, that these fields are steady in the above sense. Fig. 1 shows the dependence of the energy E of these fields on the parameter C_α (and some results concerning the stability of the fields which we will discuss later). Table 2 gives examples of energy distributions with respect to the Am and Sm parts.

Table 2. Energy ratios E^3/E^1 for the $\mathscr{A}1$ and $\mathscr{S}1$ solutions in models (ii) and (iii) at $C_\alpha = 15$

	$\mathscr{A}1$	$\mathscr{S}1$
model (ii)	0.93×10^{-4}	0.92×10^{-4}
model (iii)	1.2×10^{-3}	0.87×10^{-4}

Figs. 2 and 3 present examples of field patterns in marginal states and in finite amplitude states with $C_\alpha = 15$. In the surface maps there are no significant differences between the two states. The meridional cross-sections show that the fields in the finite amplitude states are, compared to the marginal states, more concentrated near the centre of the conducting volume.

4.4. Stability

We have tested the stability of the steady fields with respect to small perturbations. Instead of investigating linearized equations

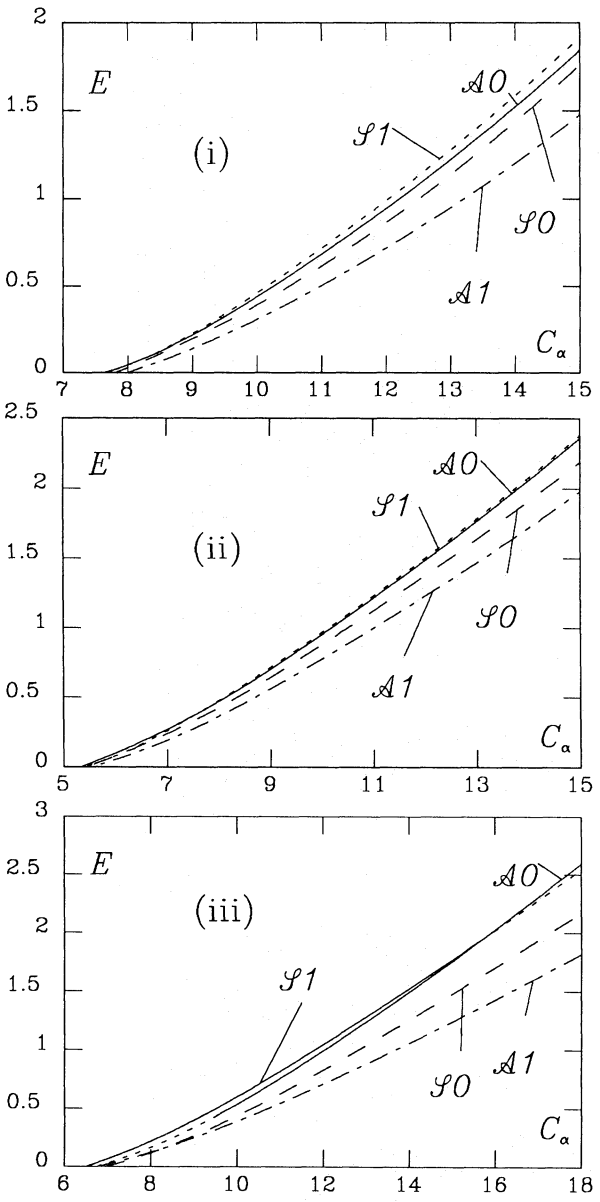

Fig. 1. The energy E (in units of $e_c R^3$) versus C_α for the steady $\mathscr{A}0$, $\mathscr{S}0$, $\mathscr{A}1$, and $\mathscr{S}1$ fields in the α^2-dynamo models (i)-(iii). In models (i) and (ii) the first bifurcation from the zero field corresponds to the $\mathscr{A}0$ field, the second to the $\mathscr{S}1$ field. For slightly supercritical values of C_α the $\mathscr{A}0$ and $\mathscr{S}1$ curves cross each other. In model (iii) the first bifurcation from the zero field corresponds to the $\mathscr{S}1$ field, the second to the $\mathscr{A}0$ field. Solid lines indicate stable solutions. In models (i) and (ii) only the $\mathscr{A}0$ solution is stable. In model (iii), for small values of C_α only the $\mathscr{S}1$ solution is stable, for $C_\alpha \gtrsim 9$ the $\mathscr{A}0$ solution becomes also stable and for $C_\alpha \gtrsim 15$ the $\mathscr{S}1$ solution becomes unstable

for the perturbations we computed the evolution of slightly perturbed steady solutions using the full nonlinear equations. As a rule, the perturbations did not consist of a simple Am or Sm part only but of several such parts. For these parts the form of the slowest free-decay modes with the corresponding symmetry was chosen.

It is possible to draw conclusions concerning the linear stability of steady fields from such results, since an arbitrary initial perturbation will contain, in general, a contribution also of that eigenmode of the linearized equation for the perturbations which has the largest growth rate (or smallest decay rate). This mode will dominate over all the others after some time and this leads to an exponential growth (or decay) of the energy of the perturbation as long as the perturbation remains small enough. The growth rate can be easily obtained from a logarithmic representation. Since we are able to consider the energies of the Am and Sm parts separately it is possible to determine the symmetry type of this dominating perturbation mode.

It should be noted that it is not justified, in general, to extract linear growth rates of other modes than the dominating one from these calculations. The nonlinear mode coupling can lead to an enslavement of modes already in the regime of a linear growth of the dominating mode. This can result in an anomalously large growth of slaved modes which has nothing to do with their own linear growth rates; see Fig. 4.

With model (i) only a few stability tests of that kind have been carried out. We recall the result of Brandenburg et al. (1989a) according to which in this model not only the steady $\mathscr{A}0$ solution but, apart from a certain neighborhood of the trivial solution, also the $\mathscr{S}0$ solution is stable with respect to axisymmetric perturbations. For the very similar model (ii) Rädler and Wiedemann (1989) found the same result. They showed, however, in addition, that the $\mathscr{S}0$ solution is no longer stable if non-axisymmetric perturbations are admitted. Then S1 perturbations grow. The main purpose of our tests with model (i) was to reconsider the stability of the $\mathscr{S}0$ solution in this sense. In order to test the stability of a solution we have added to the solution a small perturbation of another symmetry type. The result presented in the lower panel of Fig. 5 demonstrates that indeed in model (i) too the $\mathscr{S}0$ solution is unstable with respect to non-axisymmetric perturbations. Also the stability of the $\mathscr{S}1$ solution has been tested by adding an axisymmetric perturbation. The upper panel of Fig. 5 shows that such axisymmetric perturbations grow.

With models (ii) and (iii) more systematic and comprehensive stability tests with small perturbations have been carried out. As indicated in Fig. 1, in model (ii) again the $\mathscr{A}0$ solution proves to be stable. In this model again the $\mathscr{S}1$ solution is unstable with respect to A0 perturbations, and so is the $\mathscr{S}0$ solution with respect to S1 perturbations. In Fig. 6 some examples are given of the evolution of the energy ratios E_A^m/E and E_S^m/E in perturbed $\mathscr{A}0$, $\mathscr{S}0$, $\mathscr{A}1$, and $\mathscr{S}1$ solutions.

With model (iii), in which the S1 mode dominates in the linear regime, the situation is more complex. In a range of small C_α ($C_\alpha \lesssim 9$) only the $\mathscr{S}1$ solution is stable. In some range of moderate C_α ($9 \lesssim C_\alpha \lesssim 15$), however, both the $\mathscr{S}1$ and $\mathscr{A}0$ solutions prove to be stable. For larger C_α ($C_\alpha \gtrsim 15$) the $\mathscr{S}1$ solution becomes unstable and, as in models (i) and (ii), only the $\mathscr{A}0$ solution remains stable. In the first range of C_α we may expect that any solution, with arbitrary initial conditions, approaches a steady $\mathscr{S}1$ solution, and in the third range a steady $\mathscr{A}0$ solution. In the second range, however, depending on the initial conditions, a solution can evolve towards a steady $\mathscr{S}1$ or a steady $\mathscr{A}0$ solution.

4.5. Evolution for mixed initial conditions in model (i)

In addition to the investigations described so far we have carried out a number of experiments with initial fields deviating considerably from steady fields. Fig. 7 shows evolutionary tracks

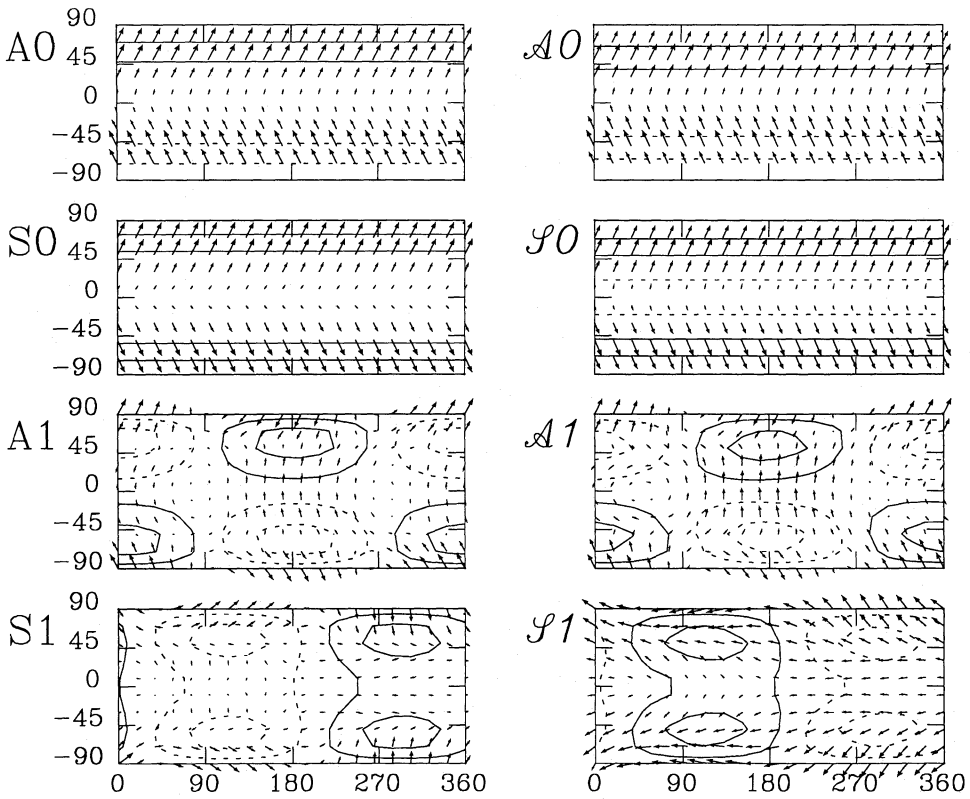

Fig. 2. Surface maps of the steady $\mathscr{A}0$, $\mathscr{S}0$, $\mathscr{A}1$, and $\mathscr{S}1$ fields in model (i), at $x = 0.95$, in the marginal state (right-hand side) and in the finite amplitude state with $C_\alpha = 15$ (left-hand side). The maps contain contours of constant B_r, where solid or broken lines correspond to positive or negative signs, respectively, and arrows indicating the (B_θ, B_ϕ)-vectors in the $\theta\phi$-plane. Note that a shift of the configurations along the ϕ-axis is without physical meaning. There are no clear differences perceptible between the fields of marginal and supercritical states

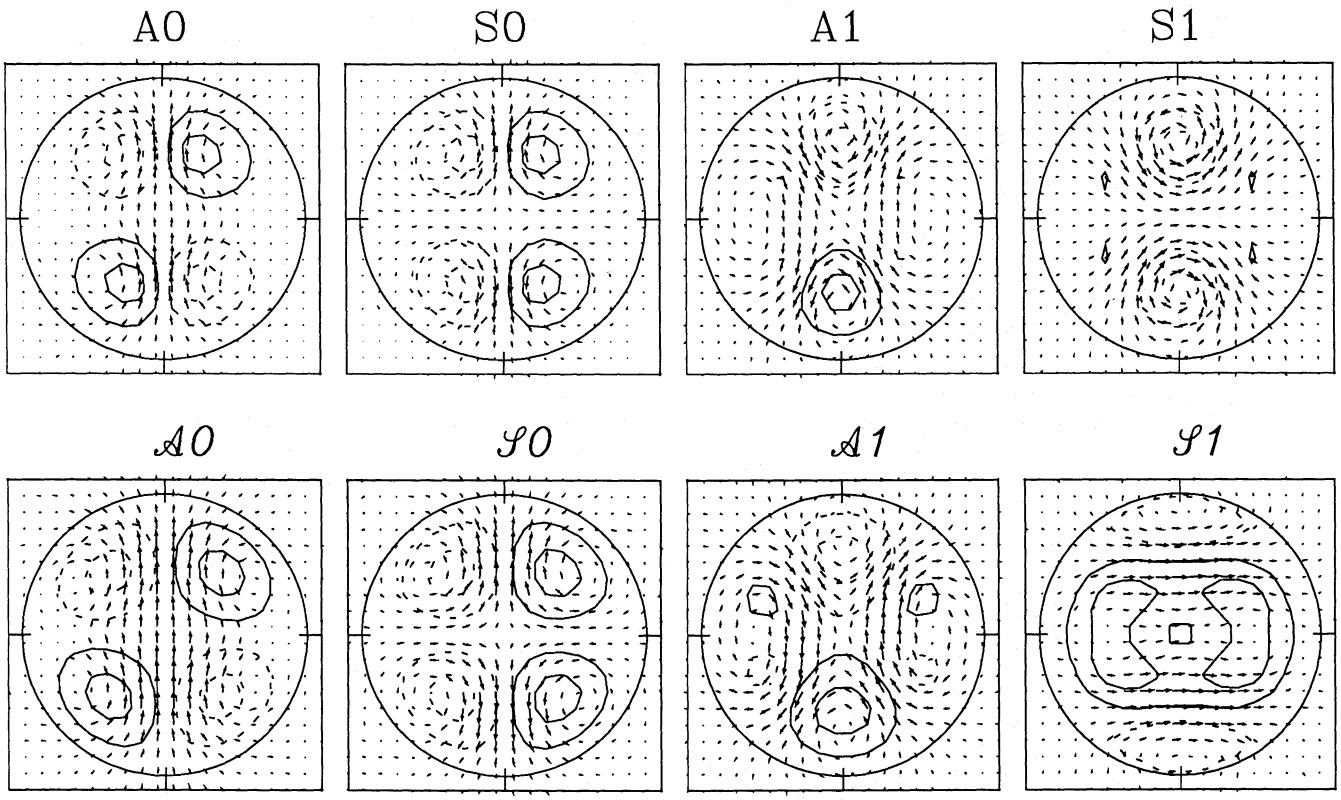

Fig. 3. Meridional cross-sections of the steady $\mathscr{A}0$, $\mathscr{S}0$, $\mathscr{A}1$, and $\mathscr{S}1$ fields in model (i) in the marginal state (upper panels) and in the finite amplitude state with $C_\alpha = 15$ (lower panels). Contours of constant B_ϕ-field are plotted together with an array of (B_r, B_θ)-vectors. The cross-sections are taken at those longitudes where the B_r-component, at $x = 0.95$, achieves a positive maximum (see Fig. 2). The finite amplitude states show typically stronger field at the centre than the marginal states

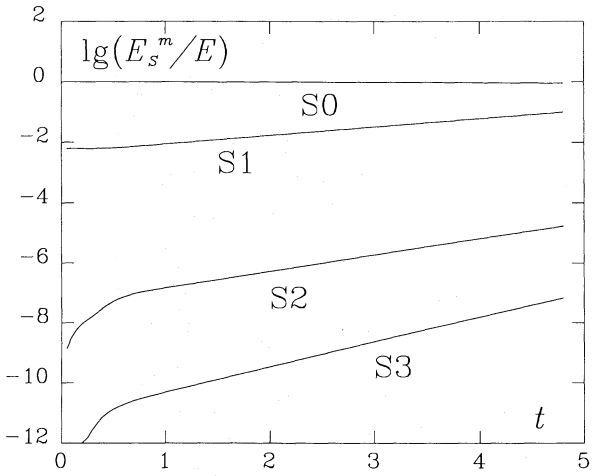

Fig. 4. Variation of the energy ratios E_S^m/E of the Sm parts after introducing an S1 perturbation to the steady $\mathscr{S}0$ solution of model (i) with $C_\alpha = 10$. Note that after a short time energy is fed also into the S2 and S3 parts. Only the growth rate of the S1 perturbation can be evaluated from the slope in the diagram since higher modes are enslaved by the growing S1 perturbation

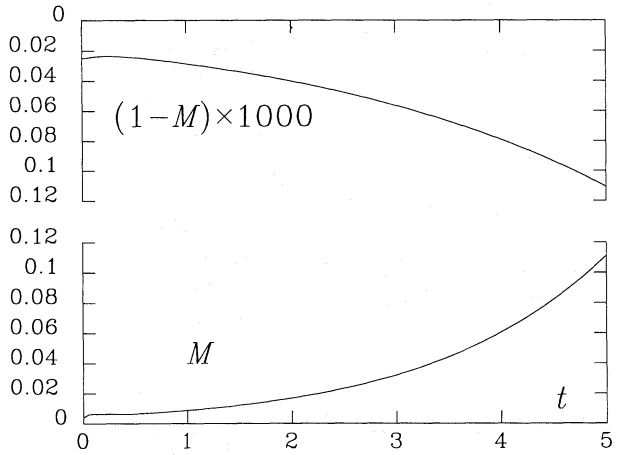

Fig. 5. Evolution of M for perturbed $\mathscr{S}0$ and $\mathscr{S}1$ solutions in model (i) with $C_\alpha = 10$. The lower panel shows that non-axisymmetric perturbations grow on the $\mathscr{S}0$ solution and the upper panel shows that axisymmetric perturbations grow on the $\mathscr{S}1$ solution. Note that the time scale of the instability for the $\mathscr{S}0$ solution is about 1000 times bigger than for the $\mathscr{S}1$ solution

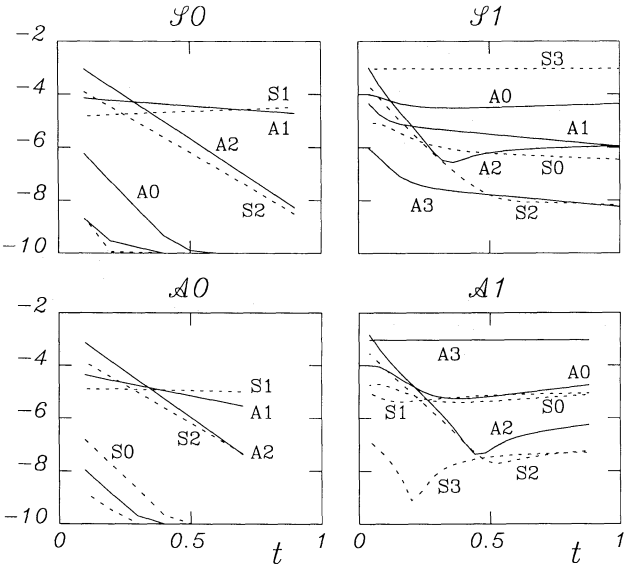

Fig. 6. The time dependence of $\lg(E_{A,S}^m/E)$ for perturbed $\mathscr{A}0$, $\mathscr{S}0$, $\mathscr{A}1$, and $\mathscr{S}1$ solutions for model (ii) with $C_\alpha = 15$. Only for the $\mathscr{A}0$ solution are the energies of all parts (apart from A0) decaying. For the $\mathscr{S}0$ solution are S1 perturbations growing, whilst for $\mathscr{A}1$ and $\mathscr{S}1$ it is the A0 mode which grows

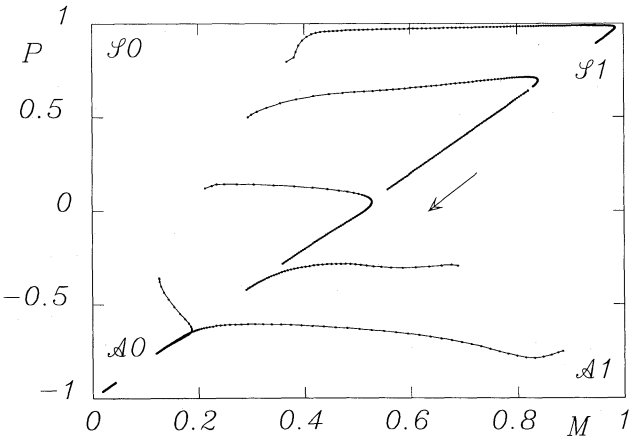

Fig. 7. $P \sim M$ diagram showing the tracks of solutions with mixed initial conditions for model (i) with $C_\alpha = 10$. The solutions at first approach the diagonal. Then the solutions turn towards $\mathscr{A}0$. The dots superimposed on the tracks mark time intervals of 0.05 diffusion times. The migration speed is very slow both near the $\mathscr{A}0$ and $\mathscr{S}1$ corners compared to other parts of the diagram

of such solutions in a $P \sim M$ diagram. In this diagram pure $\mathscr{S}0$ and $\mathscr{A}0$ solutions are located in the upper-left and lower-left corner. Non-axisymmetric solutions of S and A parity, e.g. $\mathscr{S}1$ and $\mathscr{A}1$ solutions, are on the upper-right and lower-right edge. It becomes evident from Fig. 7 that, in general, the solutions first approach the diagonal ($P = 2M - 1$). However, apart from the $\mathscr{A}0$ solution there is no other stable solution on the diagonal and the solution evolves slowly along the diagonal towards the $\mathscr{A}0$ solution. We see furthermore that for nearly axisymmetric initial conditions with $P \approx +1$ (close to $\mathscr{S}0$) the diagonal is not reached directly. The solution approaches first the line $P = 1$ and evolves then along this line towards $\mathscr{S}1$. After approaching $\mathscr{S}1$ an evolution along the diagonal begins towards $\mathscr{A}0$. The whole time span covered by the uppermost curve in Fig. 7 is about 16 diffusion times. One may estimate that the time needed to reach finally the stable $\mathscr{A}0$ solution is about 50 diffusion times.

It is interesting to note that just the same result concerning the evolution of perturbed $\mathscr{S}0$ solutions was already obtained by Krämer (1989).

The evolution of fully mixed dynamo solutions may be discussed with the help of Fig. 8 showing a "potential" surface in the $P \sim M$ diagram. It is suggested that the system evolves always along the negative gradient direction on this surface. The small hill between $\mathscr{A}0$ and $\mathscr{S}0$ in that diagram corresponds to the "watershed" found in the purely axisymmetric case (Bran-

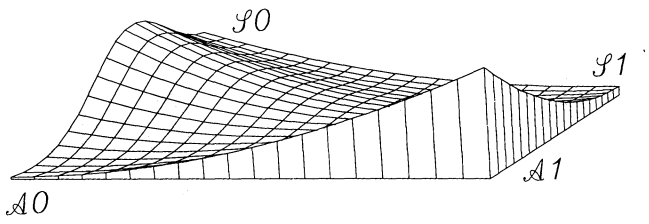

Fig. 8. A sketch of a "potential" suggested by the evolutionary tracks in the $P \sim M$ diagram of Fig. 7. It illustrates in particular the existence of a watershed between $\mathscr{A}0$ and $\mathscr{S}0$ when only axisymmetric solutions are permitted, and the possibility of a transition from $\mathscr{S}0$ to $\mathscr{A}0$ via non-axisymmetric states

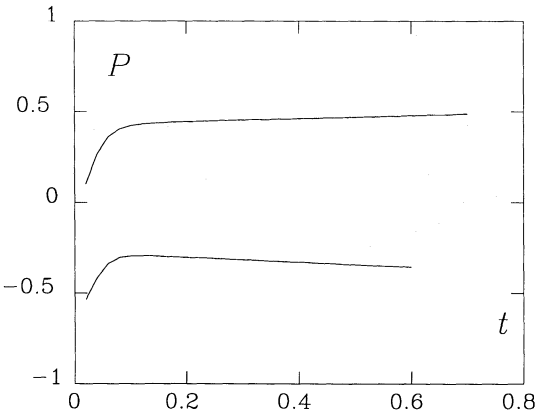

Fig. 9. $P(t)$-diagram for solutions of model (iii) with $C_\alpha = 10$. The solutions contain initially only A0 and S1 parts. There seems to be a watershed at $P \approx 0$

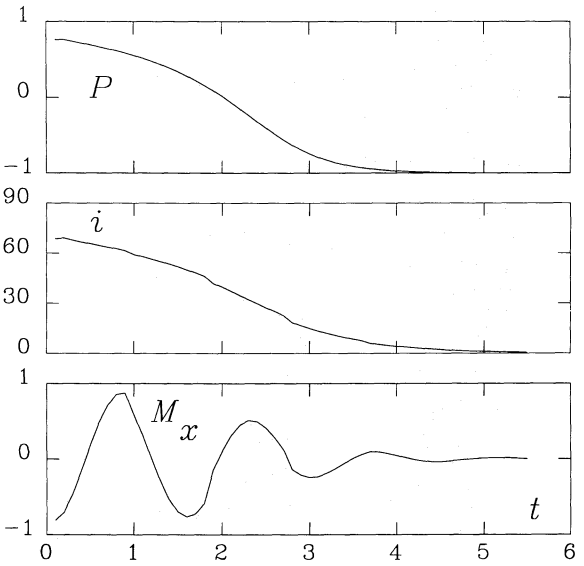

Fig. 10. Evolution of a solution containing initially only A0 and S1 parts in model (iii) with $C_\alpha = 15$. In the initial state was $P \approx 0.88$ and $Q = 1$. The $P(t)$ diagram demonstrates the evolution towards a state with $P = -1$. In this evolution the inclination angle i of the dipole axis against the rotation axis tends to zero, and the component M_x of the magnetic moment with respect to a fixed direction in the equatorial planes dies out in an oscillatory way

denburg et al., 1989a). However, if non-axisymmetric solutions are admitted the $\mathscr{A}0$ solution can be accessed from $\mathscr{S}0$ via a transient state near $\mathscr{S}1$. Although our "potential" provides some qualitative picture of the situation it is by no means clear whether a quantity of this kind can be rigorously defined.

4.6. Evolution for mixed initial conditions in model (iii)

A remarkable feature of model (iii) is that, for certain values of C_α ($9 \lesssim C_\alpha \lesssim 15$), there exist two stable solutions. Here we consider this situation in more detail.

As expected there is a watershed between $\mathscr{A}0$ and $\mathscr{S}1$ solutions. We have investigated the evolution of solutions containing initially only A0 and S1 parts. In Fig. 9 results for $C_\alpha = 10$ are given with two different initial conditions corresponding to $P = 0$ and $P = -0.6$. The solutions develop slowly towards states with $P = 1$ and $P = -1$, that is, towards $\mathscr{A}0$ and $\mathscr{S}1$ solutions, respectively.

For $C_\alpha = 15$ the basin of attraction for the $\mathscr{A}0$ solution is already very large. In the example considered in Fig. 10, in which the field again contains initially only A0 and S1 parts, the evolution leads from an initial state with $P = 0.88$ to a state with $P = -1$. In the uppermost panel of Fig. 10 we show the variation of P. The field configuration is during the whole time of dipole type, i.e. $Q = 1$. It is then natural to display also the inclination angle i of the dipole axis against the rotation axis and the component M_x of the magnetic moment with respect to a fixed direction in the equatorial plane. Clearly, M_x dies out in an oscillatory way, indicating the rotation of the field configuration. In Fig. 11 and 12 we show snapshots of the field configuration at various instants. The surface maps illustrate the passing by of two "active longitudes" during the field evolution. Finally, in the last frame, these active longitudes have disappeared. The meridional cross-sections show the variation of the field from $\mathscr{S}1$ to $\mathscr{A}0$ type.

5. Models with differential rotation

Compared to the situation with pure α^2-dynamos the behaviour of magnetic fields in the presence of differential rotation is quite different. With the restriction to axisymmetry stable mixed-parity solutions have been found (Brandenburg et al., 1989b). It is therefore interesting to study similar cases, but allowing also non-axisymmetric fields.

We have first computed an axisymmetric solution for an $\alpha\omega$-model in which α_0 is given by (21) and (22), and $\Omega = \Omega_0 x$, where Ω_0 is a constant and x as above the dimensionless radius. We were particularly interested in the parameter regime where "mixed-parity" solutions have been previously found using a gridpoint method. This was the case for $C_\alpha = 0.9$ and $C_\Omega \equiv \Omega_0 R^2/\eta = -10^4$. Details of this solution, for example the frequency ratio between long-term and short-term oscillations, are sensitive to the computational resolution. For reliable results 50 grid points in the r-direction and 100 in the θ-direction proved to be necessary. We were able to reproduce the same result with the modal method described above using $n_e = l_e = 12$ and $i_x = i_\theta = 30$. However, the time step had also to be short enough in order to achieve a sufficiently high accuracy. Good agreement was obtained when one period was covered by hundred time steps. In Fig. 14 we have plotted the evolution of the total energy

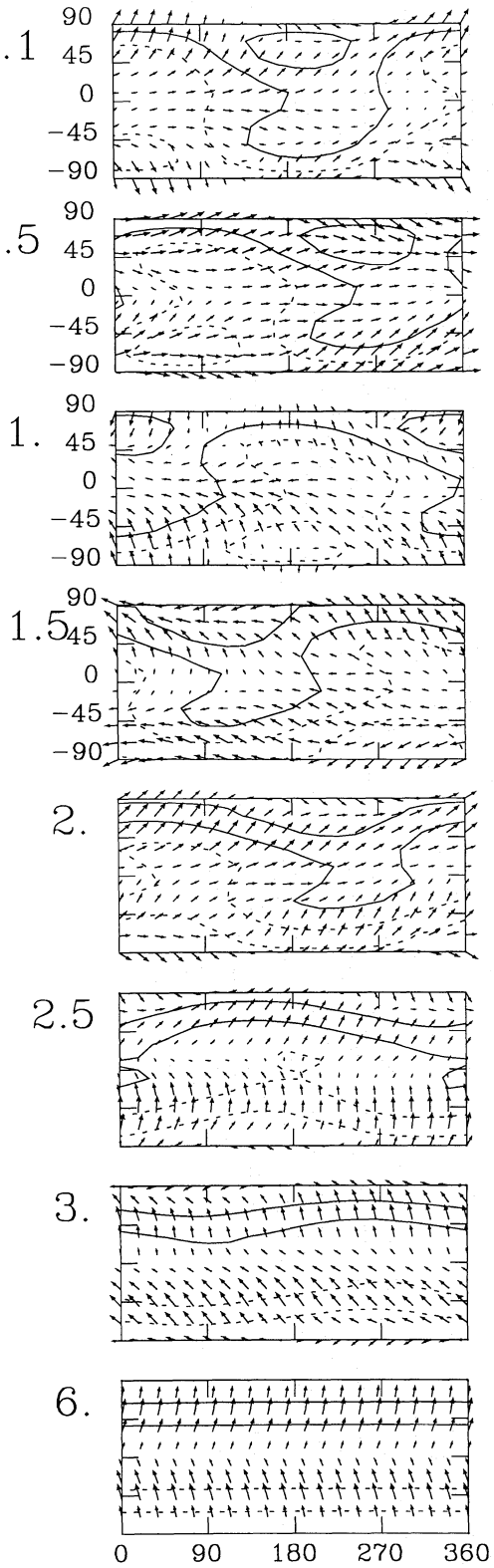

Fig. 11. Surface maps showing the magnetic field evolution, at $x = 0.95$, for the example considered in Fig. 10. The times are given in the upper left corner of each diagram. For further explanations see Fig. 2

E and the parameter P obtained with the gridpoint method and with the modal method.

For non-axisymmetric solutions a new complication arises. The presence of rotation introduces short time scales of the order of Ω^{-1} that have to be resolved. Furthermore, when field lines of a non-axisymmetric field are wound up, lines of opposite orientation occur close together and thus a short length scale arises (Rädler, 1986b). This prevented us from investigating models with such large values of C_Ω in the non-axisymmetric case. We note, however, that Jennings et al. (1990) found an axisymmetric mixed parity solution for $C_\Omega = -10^3$. Using linear stability analysis they showed that this solution is stable to non-axisymmetric perturbations. This is not so surprising, because the winding up of field lines associated with the large value of C_Ω causes the marginal dynamo numbers for non-axisymmetric modes to be very high. Thus we expect the mixed parity solution with $C_\Omega = -10^4$ also to be stable.

For further investigations we adopted a model studied by Rädler (1986a, Fig. 19), in which for moderate values of C_Ω comparable excitation conditions occur for axisymmetric and non-axisymmetric fields. The α_0-profile is defined by (21) and (23) with $x_\alpha = 0.5$ and $d_\alpha = 0.1$. The Ω-profile is given by

$$\Omega = \Omega_0 \begin{cases} -1, & \text{for } \xi_\Omega \le -1, \\ -\frac{1}{2}(1 - \frac{3}{2}\xi_\Omega + \frac{1}{2}\xi_\Omega^3), & \text{for } |\xi_\Omega| \le 1, \ \xi_\Omega = \frac{x - x_\Omega}{d_\Omega}, \\ 0, & \text{for } \xi_\Omega \ge 1, \end{cases} \quad (28)$$

with $x_\Omega = 0.8$ and $d_\Omega = 0.1$. For $C_\Omega = -300$ the marginal dynamo numbers of the A0, S0, A1, and S1 modes are very close together. For this case we have studied the stability of a solution with $C_\alpha = 3$ and a mixed initial condition which corresponds to a perturbed $\mathscr{S}1$ solution. Some results are depicted in Fig. 14. The solution evolves at first towards $\mathscr{A}0$ without reaching it and then returns to the neighborhood of $\mathscr{S}1$. This evolution is mainly along the diagonal in the $P \sim M$ diagram. Remarkably, even after returning to the neighborhood of $\mathscr{S}1$ the solution shows periodic variations in the energies of the Am and Sm parts. Unfortunately, our computational resources were not large enough to look for a final state.

6. Conclusions

In the examples investigated of α^2-dynamos with isotropic α-effect only one stable solution has been found, which is an $\mathscr{A}0$ solution. The watershed between the $\mathscr{A}0$ and $\mathscr{S}0$ solutions observed under restriction on axisymmetric magnetic fields disappears when non-axisymmetric fields are allowed. Independent of the initial conditions the final solution is of $\mathscr{A}0$ type. It is remarkable that the evolution starting from $\mathscr{S}0$ goes via an intermediate state close to $\mathscr{S}1$ and the final solution is reached only after many diffusion times.

Interesting situations can occur for dynamos with anisotropic α-effect. Depending on the dynamo number, either the $\mathscr{S}1$ or $\mathscr{A}0$ solution, or both, are stable. However, no stable mixed-parity solutions were found. The degree of anisotropy considered here is *not* unrealistically large. This model may therefore well be applicable to stars with deep convection zones and negligible differential rotation. Suppose the angular velocity of the star decreases during its evolution, and so the strength of the α-effect. We may then eventually expect a change of the field configuration

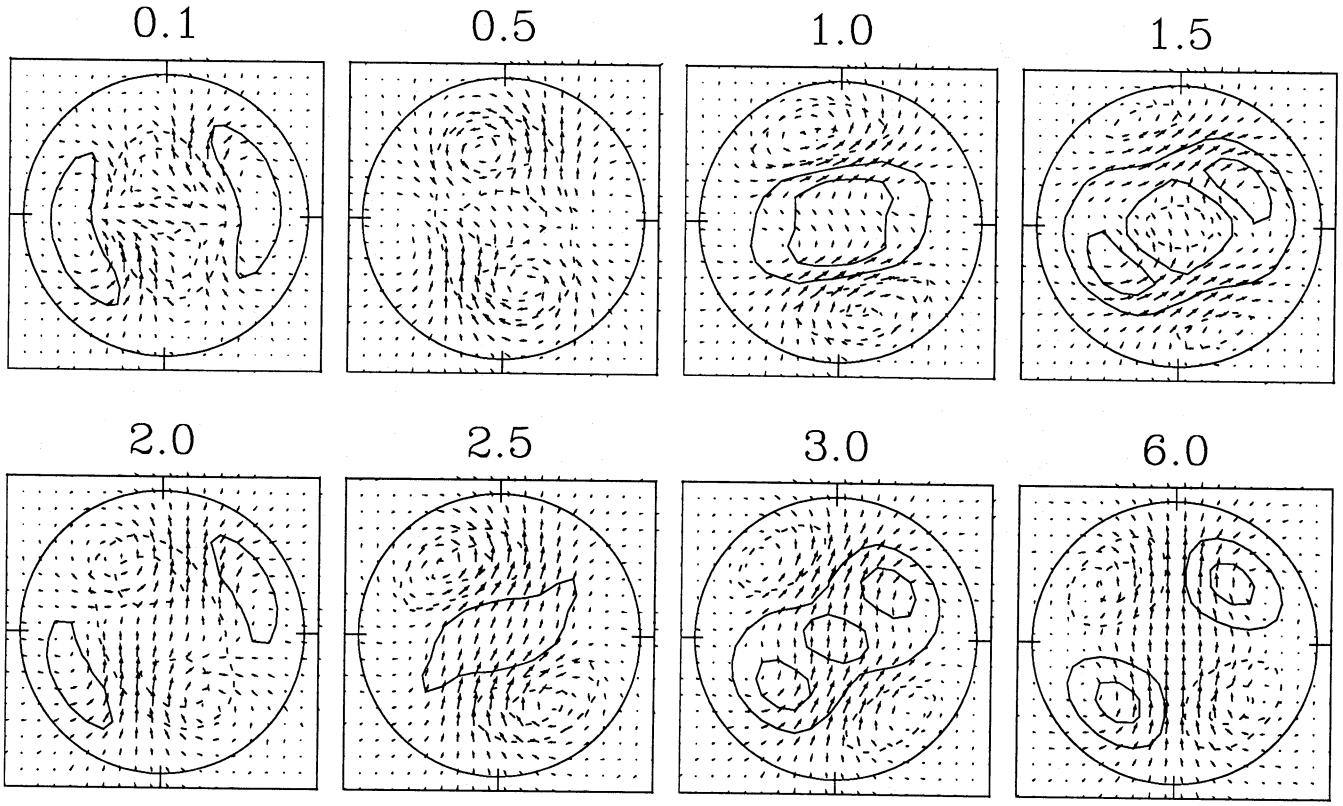

Fig. 12. Meridional cross-sections showing the field geometry for the example considered in Fig. 10. The times are given on top of each diagram. The cross-sections are taken again at those longitudes where the B_r-component, at $x = 0.95$, achieves a positive maximum (see Fig. 11)

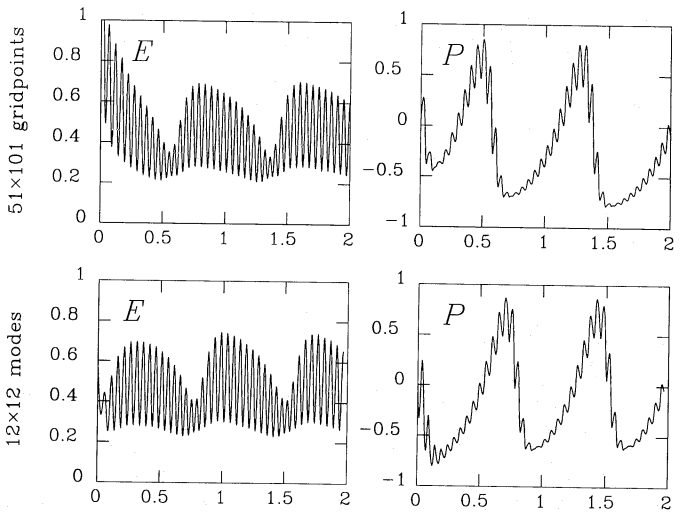

Fig. 13. The evolution of E and P for an $\alpha\omega$-dynamo, obtained with the gridpoint method (upper row; Brandenburg et al., 1989a) and with the modal method (lower row; the present paper)

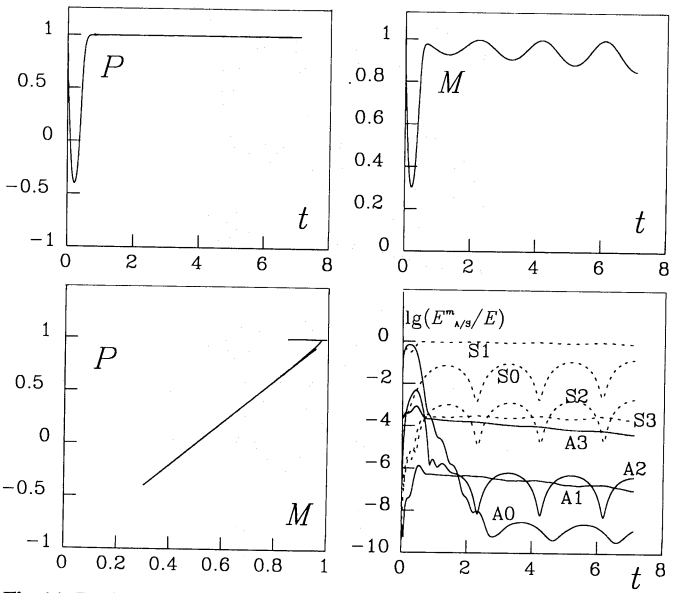

Fig. 14. Evolution of a mixed solution in an $\alpha\omega$-model with $C_\alpha = 3$ and $C_\Omega = -300$, starting from a perturbed $\mathscr{S}1$ solution. There are transient states at $t \approx 0.2$ with strongly reduced values of P and M. As can be seen from the $P \sim M$ diagram the solution evolves at first towards $\mathscr{A}0$ and then back to the neighborhood of $\mathscr{S}1$. After this a tendency towards $\mathscr{S}0$ occurs. Note the oscillatory behaviour of the energies of some parts of the field

from $\mathscr{A}0$ to $\mathscr{S}1$. This could lead to different field configurations for similar types of stars, depending on the age of these objects.

Inclusion of differential rotation, which corresponds to the transition to an $\alpha\omega$-dynamo, can lead to oscillatory solutions. The present results suggest that mixed solutions with axisymmetic and non-axisymmetric contributions are possible. Similar long-term mixed mode oscillations were reported also by Tuominen et al. (1990) and by Jennings et al. (1990). In the latter paper, however, an approximation is used which neglects radial variations of the fields and is therefore questionable. There seems to be some similarity to the earlier results for axisymmetric dynamos (Brandenburg et al., 1989a,b) which can exhibit persistent oscillations between even and odd parity.

The observations of photometric variability and chromospheric activity indicators in active stars show strong rotational modulation, which suggest a non-axisymmetric distribution of magnetic active regions. A recent discovery is that an active giant, the FK Comae type star HD 199178 (Jetsu et al., 1990), has a (possibly aperiodic) variation with a characteristic time of about 3 years in the amplitude of the photometric rotational modulation and, in addition, a 9 year photometric cycle in the mean brightness. The rotational modulation has retained its phase coherence over 13 years of observations, suggesting the presence of a persistent non-axisymmetric magnetic configuration. In another active giant, HD 32918, a snapshot of the surface structure derived by using a regularization method to invert the variable spectral line data to a temperature map has revealed a large group of cool spots in the equatorial belt, concentrated at an "active longitude" (Piskunov et al., 1990). It is tempting to describe these structures in terms of a mixed solution of the nonlinear dynamo, including, for example, A0, S0, and S1 contributions.

The solution presented in Fig. 14 is of course only one single example. The axisymmetric contribution to this solution is quite small and the variation of the strength of non-axisymmetric contributions, indicated by M, is weak but still growing. In contrast, the strong variation of the light curve modulation found by Jetsu et al. (1990) suggests a much larger influence on M. However, a closer comparison with observed stars and their interpretation in terms of certain dynamo models is at present not yet justified. Other parameter values and inclusion of dynamical effects may reveal a more complex behaviour.

References

Braginski, S. I.: 1970, *Geomagn. Aeron.* **10**, 1

Brandenburg, A., Krause, F., Meinel, R., Moss, D., Tuominen, I.: 1989a, *Astron. Astrophys.* **213**, 411

Brandenburg, A., Moss, D., Tuominen, I.: 1989b, *Geophys. Astrophys. Fluid Dyn.* **49**, 129

Ivanova T. S., Ruzmaikin, A. A.: 1977, *Sov. Astron.* **21**, 479

Jennings, R., Brandenburg A., Moss, D., Tuominen I.: 1990, *Astron. Astrophys.* **230**, 463

Jepps, S. A.: 1975, *J. Fluid Mech.* **67**, 625

Jetsu L., Huovelin J., Tuominen I., Vilhu O., Bopp B. W., Piirola V.: 1990, *Astron. Astrophys.* (in press)

Kleeorin, N. I., Ruzmaikin, A. A.: 1984, *Astron. Nachr.* **305**, 265

Krause, F., Meinel, R.: 1988, *Geophys. Astrophys. Fluid Dyn.* **43**, 95

Krämer, A.: 1989, *GAMMA* **48**, Diploma thesis, Tech. Univ. Braunschweig

Piskunov N.E., Tuominen I., Vilhu O.: 1990, *Astron. Astrophys.* **230**, 363

Rädler, K.-H.: 1984, *Astron. Nachr.* **305**, 289

Rädler, K.-H.: 1986a, *Astron. Nachr.* **307**, 89

Rädler, K.-H.: 1986b, *Plasma Physics*, ESA SP-251, 569

Rädler, K.-H., Wiedemann, E.: 1989, *Geophys. Astrophys. Fluid Dyn.* **49**, 71

Rüdiger, G.: 1973, *Astron. Nachr.* **294**, 183

Rüdiger, G.: 1974, *Astron. Nachr.* **295**, 275

Stix, M.: 1972, *Astron. Astrophys.* **20**, 9

Tuominen, I., Piskunov, N. E., Moss, D., Brandenburg, A.: 1990, in *Sixth Cambridge Workshop on Cool Stars, Stellar Systems, and the Sun* (in press)

This article was processed by the author using Springer-Verlag TEX AA macro package 1989.